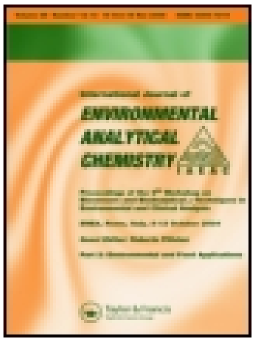

International Journal of Environmental Analytical Chemistry

ISSN: (Print) (Online) Journal homepage: https://www.tandfonline.com/loi/geac20

Degradation of methylene blue and methyl violet using graphene oxide/NiO/β-cyclodextrin nanocomposites as photocatalyst

Ranjana Dewangan , Ayesha Hashmi , Anupama Asthana , Ajaya K. Singh & Md Abu Bin Hasan Susan

To cite this article: Ranjana Dewangan , Ayesha Hashmi , Anupama Asthana , Ajaya K. Singh & Md Abu Bin Hasan Susan (2020): Degradation of methylene blue and methyl violet using graphene oxide/NiO/β-cyclodextrin nanocomposites as photocatalyst, International Journal of Environmental Analytical Chemistry, DOI: 10.1080/03067319.2020.1802443

To link to this article: https://doi.org/10.1080/03067319.2020.1802443

INTERNATIONAL JOURNAL OF ENVIRONMENTAL ANALYTICAL CHEMISTRY
https://doi.org/10.1080/03067319.2020.1802443

Taylor & Francis
Taylor & Francis Group

ARTICLE

Degradation of methylene blue and methyl violet using graphene oxide/NiO/β-cyclodextrin nanocomposites as photocatalyst

Ranjana Dewangan[a], Ayesha Hashmi[a], Anupama Asthana[a], Ajaya K. Singh[a] and Md Abu Bin Hasan Susan[b]

[a]Department of Chemistry, Govt. V. Y. T. PG. Autonomous College, Durg, India; [b]Department of Chemistry, University of Dhaka, Dhaka, Bangladesh

ABSTRACT

We report the synthesis of graphene oxide/nickel oxide/β-cyclodextrin (GO/NiO/β-CD) nanocomposite and the efficiency of the nanocomposite in decolourising two different dyes, methylene blue (MB) and methyl violet (MV). GO was prepared by modified Hummer's method while hydrothermal method was used for the preparation of GO/NiO/β-CD. The as-synthesised nanocomposites were characterised by X-ray diffraction (XRD), and Fourier transform infrared (FTIR) spectroscopy, Raman spectroscopy and high resolution transmission electron microscopy (HR-TEM). Photocatalytic degradation was carried out under solar light by monitoring the concentration of MB and MV dyes. Degradation reaction followed Langmuir-Hinshelwood pseudo first-order kinetic model. The apparent reaction rate constant (k) for MB increased as compared to MV under solar light irradiation. The MB showed better photocatalytic degradation efficiency by GO/NiO/β-CD composites. GO/NiO/β-CD nanocomposite has been very favourable for photocatalytic application.

ARTICLE HISTORY
Received 5 March 2020
Accepted 15 July 2020

KEYWORDS
GO; GO/NiO; GO/NiO/β-CD; photocatalyst; photodegradation; kinetic model

1. Introduction

The modern era experiences rapid industrialisation with rise in textile industries and consequent uses of dyes. According to a World Bank report, almost 20% of global industrial water pollution comes from the dyeing industries and finishing processes of textiles [1]. A variety of organic dyes have been widely used for a long time in many industrial fields, such as paper making, coating and textiles [2]. Organic dyes are harmful because of their stable structures and their by-products have caused a mutagenic or carcinogenic impact on human beings as well as aquatic life. The discharge of stable and carcinogenic dyes into water bodies are harmful to human health, and cause illness such as cholera, diarrhoea, precordial pain, dizziness, abdominal pain, bladder irritation, staining of skin etc [3]. Dyes also affect aquatic life by hindering the photosynthesis process of aquatic plants, eutrophication and perturbation [4–6]. Therefore, much attention should be paid to treat dyes before their discharge [6].

CONTACT Anupama Asthana anurakeshbhilai@gmail.com; Ajaya K. Singh ajayaksingh_au@yahoo.co.in

Supplemental data for this article can be accessed here

Numerous techniques, such as activated carbon adsorption (physical method), chlorination (chemical method) [7], and aerobic biodegradation (biochemical method) [8,9], liquid-liquid extraction, membrane filtration and adsorption [10] have been generally applied to treatment and separation of dyes from textile wastewater [11]. However, advanced treatments are required for breakdown of parental cationic dyes to benzene, NO_2, CO_2 and SO_2 which may cause secondary pollution in the environment [12]. Advanced oxidation processes (AOPs) are one of the widely used method, applied to mineralise dyes into CO_2 and H_2O [13,14]. AOPs are more reliable when associated with aspects like, ozonation, photolysis, and photocatalysis with support of oxidants, light, and semiconductors. Photocatalytic degradation is initiated when the photocatalysts absorb photons (UV) to generate electron-hole pairs on the catalyst surface [15,16]. The positive hole in the valence band ($h_{VB}{}^{+}$) will react with water to form hydroxyl radical (*OH), followed by the oxidation of pollutants to CO_2 and H_2O [17,18].

MB and MV both are cationic azo dyes in nature. MB is also known as basic blue 9. Both are widely used in textile industries for dye processing and up to 50% of the dyes are consumed in textile industries and also used in dyeing of wool, cotton and so on [19,20]. This colour can cause harmful effects like dyspnoea, skin irritation, heart palpitations and seizure on humans. Therefore, it is essential to remove the existing industrial waste water. In the past few years, several catalysts such as TiO_2 [21], $BiFeO_3$ [22], ZnS [23] and ZnO [24] have been used to degrade MB and MV (Table S1).

Graphene and GO based nanocomposites have attracted noteworthy attention due to their many excellent properties such as mechanical flexibility, chemical stability and large surface area. GO based nanocomposites can serve for dye removal in aqueous solution. Apart from this, its high valence band in comparison to anatase and rutile phase inhibits hole transfer, thereby increases the photocatalytic efficiency. In comparison to the traditional materials such as traditional 2D electron gas (2DEG), the GO is much thinner. A 2DEG in a heterostructure has an average thickness of ~5–50 nm, while GO, in contrast, is a single layer of carbon atom and has the thickness of ~3 Å. The thin foldable sheet like structure of GO also gives an opportunity to wrap it like a cloth on different nanoparticles. The resulting nanocomposite may show enhanced photocatalytic properties due to the tightly bonded structure giving rise to the synergistic or additional effect [25]. GO, with its unique electronic properties and high transparency, contributes to facile charge separation and is adsorptive in its structure as a potential photocatalytic material [26]. Similarly, NiO is a p-type semiconductor with a wide band gap between valence and conduction band, making it specifically suitable as a photocatalyst [27]. Several methods reported for the synthesis of NiO nanostructure are: sol gel [28], precipitation [29], low pressure spray pyrolysis [30], solvothermal [31], combustion [32] and thermal decomposition [33]. Thermal decomposition of nickelous precursors, especially $Ni(OH)_2$, has commonly been employed by many researchers [34,35]. β-CD, a cyclic oligosaccharide, consists of seven α-D-glucose units connected through α-(1,4) linkages and has a hydrophobic inner cavity and a hydrophilic exterior [36]. β-CD can enable them to bind selectively various, organic and inorganic pollutant into their cavities to form stable host-guest inclusion complexes or nanostructured supramolecular assemblies in their hydrophobic cavity, showing high molecular enantioselectivity and selectivity [37]. The β-CD has the capability of forming inclusions with various compounds such as aromatic compounds by virtue of a series of weak intermolecular forces [38]. Hydrothermal method has also been attempted in preparing the nanomaterials in recent years, which offers advantages such as high purity, simplicity, variation in nanostructures, smaller and more coherent particles [39]. Considering the benefits of photocatalysis in wastewater treatment and the need for high quality, large scale NiO nanostructures, research is carried out on producing this material using calcinations of GO-based metal oxide/polymer nanocomposite prepared hydrothermally, but with the aid of a more economic stabiliser [40]. Durmus et al. highlighted that the efficiency of any metal oxide photocatalyst in heterogeneous photocatalytic reactions requires a suitable architecture that minimises electron loss during excitation state and maximises photon absorption. They emphasised the unique features of metal doping or binary composite photocatalyst system and increasing interest for such systems [41].

There have been numerous reports on synthesis and application of GO based metal oxide polymer nanocomposites as photocatalyst. Tan et al. reported the preparation of graphene/beta-cyclodextrin (GNS/β-CD) composite by an improved method and its adsorption performance for phenolphthalein was investigated. This improved method could enhance the stability of GNS/β-CD due to the covalent bond link between β-CD and GNS, and achieve the synergistic adsorption of organic dye compound on β-CD and GNS in GNS/β-CD composite because of the removal of some oxygen-containing groups on the surface of GO in GNS/β-CD [42]. Fan et al. reported synthesis of ZnO and graphene composites (ZnO/GRs) by a simple and non-toxic hydrothermal reaction route and showed that in comparison with ZnO and P25, the ZnO/GRs exhibited enhanced photocatalytic performance for degradation of methylene blue (MB) since the graphene sheets could prevent the photo-induced hole–electron pairs of ZnO from recombination by transferring the photo-induced electron to the MB. The mass ratio of ZnO to graphene was 50:1, the ZnO/GR showed the best photocatalytic performance [43]. GO intercalated montmorillonite nanocomposites were prepared by Puri et al. by a facile chemical route and were used for the adsorption of crystal violet from contaminated water. The results indicated that the synthesised nanocomposites adsorb crystal violet efficiently (~96%) with a small decrease in removal efficiency even after five cycles of adsorption and could be employed in wastewater treatment for the removal of cationic dyes [44]. Janani et al. successfully synthesised magnetically reduced graphene oxide–bismuth oxybromide (MRGO–BiOBr) composite and reported that this possesses magnetic, adsorptive and photocatalytic properties. Photocatalytic degradation of MB under visible light irradiation was examined using MRGO–BiOBr and around 96.84% of dye of 50 ppm was degraded in 2 h. Kinetic studies were performed by splitting the kinetic data into two regions at 30 min of irradiation and using the Langmuir–Hinshelwood (L–H) model to determine the rate constants [45]. Wang et al. synthesised aspartic acid-β-CD (ACD) by the reaction of β-CD with aspartic acid and epichlorohydrin, and graphene oxide-TiO_2 (GO-TiO_2) composite catalyst was prepared by a hydrothermal method. The results showed that the presence of ACD was favourable to the acceleration of photocatalytic oxidation of new coccine (NC) and photocatalytic reduction of Pb^{2+} in the single pollution system, and the photocatalytic reaction rate constants of NC and Pb^{2+} in the presence of ACD increased by 58% and 42%, respectively [46].

An efficient GO-based nanocomposite prepared by exploiting the advantageous properties of NiO and β-CD are yet to be developed for use as a photocatalyst. In this work, we therefore, report a facile method to synthesise GO/NiO/β-CD nanocomposites via hydrothermal method. Synthesised GO/NiO/β-CD nanocomposites were further characterised by XRD, Raman, FTIR and HR-TEM spectroscopy. Photocatalytic activity of GO/NiO/β-CD nanocomposite was examined by following decomposition of MB and methyl violet (MV dyes) as model compounds under sunlight. This study aims at determining the optimum experimental conditions for the best photodegradation performance of GO/NiO/β-CD nanocomposites.

2. Experimental section

2.1. Materials and reagents

Graphite powder was purchased from Sigma Aldrich. β-CD, nickel chloride (Merck), 33% hydrogen peroxide (Merck), concentrated sulphuric acid (Merck, 98% pure), potassium permanganate (Merck), ferrous sulphate (Merck), hydrochloric acid (Merck), ammonia solution (Merck), sodium hydroxide (Merck), ethanol (Merck) were used without further purification. All other chemicals were purchased from Mumbai, India Pvt. Ltd. Double distilled water was used throughout the work.

2.2. Synthesis of GO

GO was prepared according to the modified Hummer's method. 2.0 g of graphite powder was mixed with 100 mL H_2SO_4 and stirred in an ice bath for 2 h. Next, 8.0 g of $KMnO_4$ was slowly added so that the temperature of the mixture remained below 10° C. The suspension was then reacted for 2 h in an ice bath and stirred for 60 min before again being stirred in a 40°C water bath for 60 min. The temperature of the mixture was adjusted to a constant 98°C for 60 min while water was added continuously. Deionised water was further added so that the volume of the suspension was 400 mL. 20 ml of H_2O_2 (33%) was added after 5 min to reduce the unreacted oxidant until the slurry turned golden yellow. The reaction product was filtered and washed with deionised (DI) water and 5% HCl solution repeatedly. Finally, the product was dried at 60°C for 24 h [47].

2.3. Synthesis of inorganic gel of NiO

In a typical synthesis of NiO, 0.1 M of nickel chloride ($NiCl_2$) solution was prepared by dissolving it in 4.0 M HCl solution and stirred at 60°C for 15 min, then the pH was increased to ~7 by adding 2 M NaOH and stirring was continued for 2 h. The result was a greenish solution to which 20 mg of GO (previously dispersed in 40 mL of DI water by ultrasonication) wase added to assurance a complete combination of the metal ion and the oxygen-containing functional groups on the edges and surface of GO. After complete disollution, ammonia (28 wt% in water) was added drop by drop to the GO dispersion with continuous stirring for 2 h. The product formed was washed repeatedly with water and alcohol finally with acetone and dried at room temperature. The sediment was collected and dried in an oven at 45°C for 24 h to improve the crystallinity of GO/NiO nanocomposites [48].

2.4. Synthesis of GO/NiO/β-CD nanocomposites

The GO/NiO/β-CD nanocomposites were synthesised using modified GO, GO/NiO composite solution, β-CD and $FeSO_4.7H_2O$. GO/NiO was first dispersed in DI water for 10 min in an ultrasonic bath and 0.250 g of β-CD was added. 0.695 g of $FeSO_4.7H_2O$ was added to 50 mL of aqueous dispersion of GO. The DI water was used as pre-dispersing solvent because both GO and metal oxide showed good dispersion in DI water. The use of pre-dispersing solvent helps in the preparation of nanocomposites with stronger interfacial interactions among filler and polymer matrix [49]. After ultrasonic dispersion, the pH of the solution was adjusted to maintain a level of 11 by adding ammonia solution during the reaction. After the above steps, the resultant black precipitate was collected by filtration, washed with ethanol and DI water sequentially to remove excess β-CD and then, the precipitate was dried in a vacuum oven at 40ºC for 6 hrs.

2.5. Instrumentation

XRD: XRD was recorded on a Bruker AXS D8 Advance using Cu radiation at a wavelength of 1.5406 Å, and Si (Li) PSD detector was used. Temperature was controlled by Anton paar, TTK 450 in the temperature range of −170°C to +450°C. **FTIR**: FTIR spectra were recorded on a Thermo Nicolet, Avtar 370 FTIR spectrophotometer. The samples were prepared as KBr disks and spectral range was around 4000–400 cm $^{-1}$. DTGS detector was used. Resolution was set as 4 cm $^{-1}$. **Raman spectroscopy**: Raman spectra were recorded using BRUKER RFS 27 stand-alone FT-Raman. Scan range was around 50–4000 cm^{-1}, resolution was around 2 cm^{-1} and laser source was Nd:YAG 1064 nm. **HR-TEM**: HR-TEM images were recorded in a JEOL JEM 2100 microscope. Resolution was around point: 0.23 nm, lattice: 0.14 nm and magnification was 2000×, 1,500,000 ×.

3. Results and discussion

3.1. XRD

XRD patterns of GO, GO/NiO and GO/NiO/β-CD nanocomposites are illustrated in Figure 1. Pure NiO exhibits three sharp diffraction peaks at 2θ of 37°, 43° and 62° [50] . The pure β-CD gave high-intensity diffraction peaks with main diffractions at 2θ of 6.26°, 9.21°, 12.65°, 17.19° and 21.13°. The characteristic peak of GO and the emergence of β-CD characteristic peak and the change of the peak intensity fully demonstrated the successful modification of β-CD [51]. GO has a characteristic peaks at around 2θ of 10.38º, which resembles to the (001) reflection of stacked GO sheets and d-spacing is obtained around 0.968 Å. In XRD patterns of GO/NiO composite, the diffraction peaks are obtained at 2θ of 9.35º with (001) plane and d-spacing is found around 1.878 Å. The XRD pattern of GO/NiO/β-CD nanocomposites has a diffraction peak of 2θ at 9.98º, which corresponds to the (001) reflection. The d-spacing is obtained around 6.822 Å. In addition, the average grain size of GO/NiO/β-CD nanocomposites can be estimated to be 9.37 nm as calculated by using the Scherrer's formula [52].

$$D = \frac{K\lambda}{\beta \cos\theta} \tag{1}$$

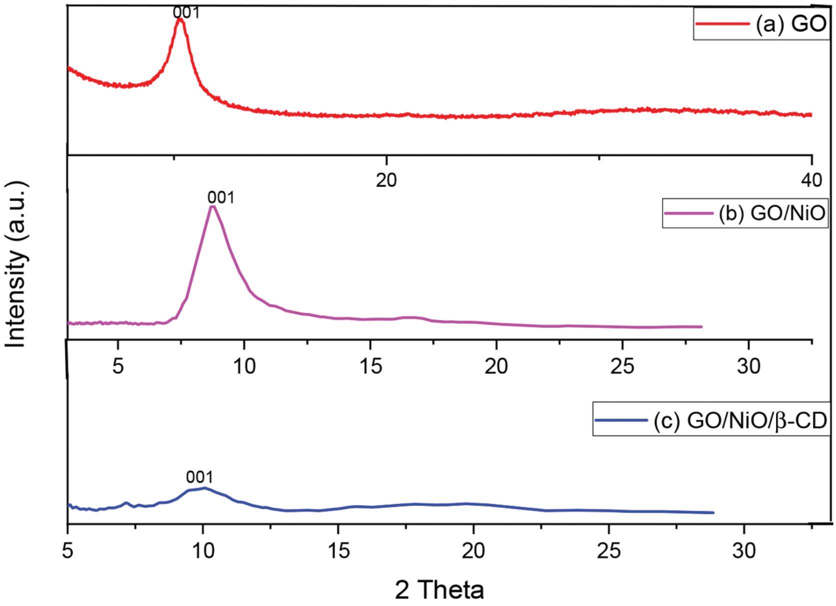

Figure 1. XRD pattern of (a) GO, (b) GO/NiO and (c) GO/NiO/β-CD.

Where, D is the average crystalline size (nm), k is a constant 0.89, λ, the wavelength of radiation source used is 1.54 Å, β is the full width of half maximum (FWHM) in radian, θ is the angle at maximum peak.

d-spacing is determined by using Bragg's equation, i.e [53].,

$$2d\sin\theta = n\lambda \tag{2}$$

Where d is the interplanar distance, λ is the wavelength of radiation source used is 1.54 Å and n is an integer. Table 1 summarises the comparison of different XRD parameters of various nanocomposites.

3.2. FTIR spectra

The qualitative aspect of infrared spectroscopy is one of the most powerful attributes of this diverse and versatile analytical technique. FTIR analysis is used to determine the functional groups present in the sample along with whether the compound is saturated or unsaturated. Figure 2 shows the FTIR spectrum of GO, GO/NiO and GO/NiO/β-CD nanocomposites. Peaks and the corresponding functional groups of pure NiO [56], β-CD [51] have been listed in Table 2.

3.3. Raman spectra

Raman spectroscopy is one of the most effective techniques to characterise the composite materials. Raman spectra of (a) GO, (b) GO/NiO and (c) GO/NiO/β-CD are shown in Figure 3. The curve of GO (Figure 3(a)) shows a D band at 2125 cm^{-1} and G band at 2209 cm^{-1}. While from Figure 3(b) the Raman spectrum of GO/NiO also shows D and

Table 1. Comparison of different XRD parameters of various nanocomposites.

Substances	2θ	hkl	Grain size	References
GO/magnetic β-CD/chitosan	30.15	220	Very small size	[54]
	36.27	311		
	43.32	400		
	53.89	422		
	57.13	511		
	62.29	440		
Magnetic GO/β-CD	30.09	220	Very small size	[67]
	35.42	311		
	37.05	222		
	43.05	400		
	53.39	422		
	56.94	511		
	62.51	440		
GO/β-CD/poly(acrylic acid)	11.1	-	0.80 nm	[68]
GO/Fe_3O_4/β-CD	30.2	220	8 nm	[55]
	35.5	311		
	43.2	400		
	53.6	422		
	57.1	511		
	62.9	440		
Magnetic GO/β-CD/poly (L-glutamic acid)	30.23	220	26 nm	[41]
	35.53	311		
	37.66	222		
	43.42	400		
	53.85	422		
	57.17	511		
	62.84	440		
Pure NiO	37	-	-	[50]
	43			
	62			
β-CD	6.26	-	-	[51]
	9.21			
	12.65			
	17.19			
	21.13			
GO	10.38	001	1.26	This work
GO/NiO	9.35	001	4.9	
GO/NiO/β-CD	9.98	001	9.37	

G bands at 2122 cm^{-1} and 2199 cm^{-1}, respectively. Similarly Raman spectrum of GO/NiO/β-CD nanocomposites (Figure 3(c)) shows a D and G band at 2125 cm^{-1} and 2128 cm^{-1} respectively. The Raman spectrum of GO/NiO/β-CD shows relative higher intensity of D to G band than that of GO. The intensity ratio (I_D/I_G) of the D band to G band in graphitic materials has been used to determine the size of sp^2 domains. The I_D/I_G ratio were 0.967 for GO, 0.968 for GO/NiO, and 0.975 for GO/NiO/β-CD. The increased I_D/I_G ratio suggested the decrease in size of sp^2 domains from GO/NiO/β-CD and further confirm formation of new graphitic domains after the reduction process [63].

3.4. HR-TEM

HR-TEM images of as-prepared nanocomposites (GO, GO/NiO, GO/NiO/β-cyclodextrin) are shown in Figure 4. Figure 4a clearly indicates the GO nanosheets resembling like extremely thin film. The resulted GO suspension is homogeneous and agglomerates together. Figure 4(b) shows that GO/NiO nanoparticles are uniform in size with spherical grains,

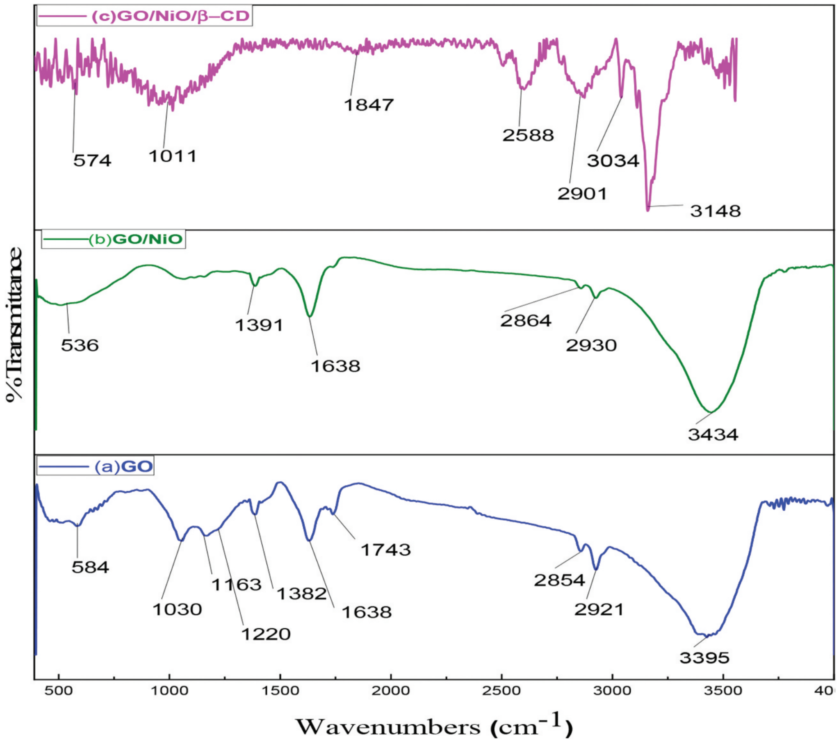

Figure 2. FTIR spectrum of (a) GO, (b) GO/NiO and (c) GO/NiO/β-CD.

which are evenly distributed on the two-dimensional graphene substrate. The NiO nanoparticles are surrounded by flexible graphene nanosheets, which can preserve the two-dimensional structure of the GO/NiO nanocomposites. Figure 4(c) clearly shows that GO sheets are the matrix of β-CD composite and wrinkles are observed on the surface of GO/NiO/β-CD, which may be important for preventing aggregation of GO, metal oxide and β-CD nanocomposites [67].

The selected area electron diffraction (SAED) pattern is useful for determining the crystallinity of the sample, Figure 4 (d), (e) and (f) indicate that the materials GO and GO/NiO, GO/NiO/β-CD are polycrystalline in nature. The intensities of all the diffraction spots are not equal and sharp enough. Moreover, the diffraction spots are associated with some unresolved spots. However, this kind of diffraction pattern may also arise from the adsorption of β-CD on the surface of GO [68].

3.5. Study of photocatalytic activity

MB, i.e. 3,7-bis-(dimethylamino)-phenothiazin-5-ium chloride) has molecular weight of 319.85 g/mol. During spectrophotometric evaluation it shows absorption maximum at 663 nm. While, MV is a cationic azo dye (Tris (4-dimethylamino)phenyl)methylium chloride) with molecular weight of 393.959 g/mol. It shows absorption maximum at 584 nm. Photocatalytic experiments were carried out by photodegradation of MB and MV using UV-Vis spectroscopy. A 96 W UV-A lamp was used as the irradiation source. A stock

Table 2. Assignments of the FTIR peaks.

Sample	Functional group	Peak (cm^{-1})	Reference
Pure NiO	Hydroxide ions should not be observed on pure NiO	3470	[56]
β-CD	O-H	3313	[51]
	C-H	2930	
	O-H bonds in the primary and secondary hydroxy group of -CD and C-H	1204,1252,1296,	
	C-O-C	1334,1366,1414,	
	C-O	1151	
	C-C	1029	
	Deformation vibration of the C H bonds and ring vibration	1077	
		569, 708, 756, 942	
GO	O-H	3395	[57]
	C = C	1743	[52]
	C-OH	1382	[58]
	Phenolic and tertiary alcohol	1220	[57]
	C-O-C	1163	[52]
	C-O	1030	[53]
	Alcohol out of plane bend Aliphatic C-H stretches	584	[52]
		2921,2854	[58]
	Stretching vibrations of COO^{-}	1638,1391	[59]
GO/NiO	Hydrophilic oxygenised functional groups	3434	[60]
	C-H	1391	[59][59]
	Ni-O	536	
GO/NiO/β-CD	O-H	3148	[61]
	C-O/C-C	1847,1011	[62]
	Suggesting the CH_n CH_2	2901	[61]
	C-O vibrations of β-CD	2588	[58]

Table 3. Comparative study of I_D/I_G ratio in Raman spectra.

Sample	I_D/I_G ratio	Reference
GO	0.86	[63]
AGO	0.89	
GR	0.79	[64]
f-GR	1.02	
MTSG-20	1.06	[65]
MTSG-10	1.07	
MTSG-5	1.06	
MTSG-1	1.11	
FGO	1.02	[66]
FGO/ZnO	1.18	
GO	0.967	This work
GO/NiO	0.968	
GO/NiO/β-CD	0.975	

Table 4. Kinetic parameters of photocatalytic degradation of MB and MV.

Dye	k^* (min^{-1})	r^2	Degradation efficiency (%)
MB	0.0076	0.975	90.00%
MV	0.0049	0.929	69.54%

solution of MB or MV (100 ppm in water) was prepared for photodegradation. In order to optimise the nanocatalyst amount for dye degradation, solutions of different concentrations were taken and their pH was adjusted at the required values. The reaction solutions were prepared by the addition of catalyst into each conical containing dye solutions. An appropriate amount of catalyst (0.1–0.8 g dose) was suspended into 20 ppm of MB or MV

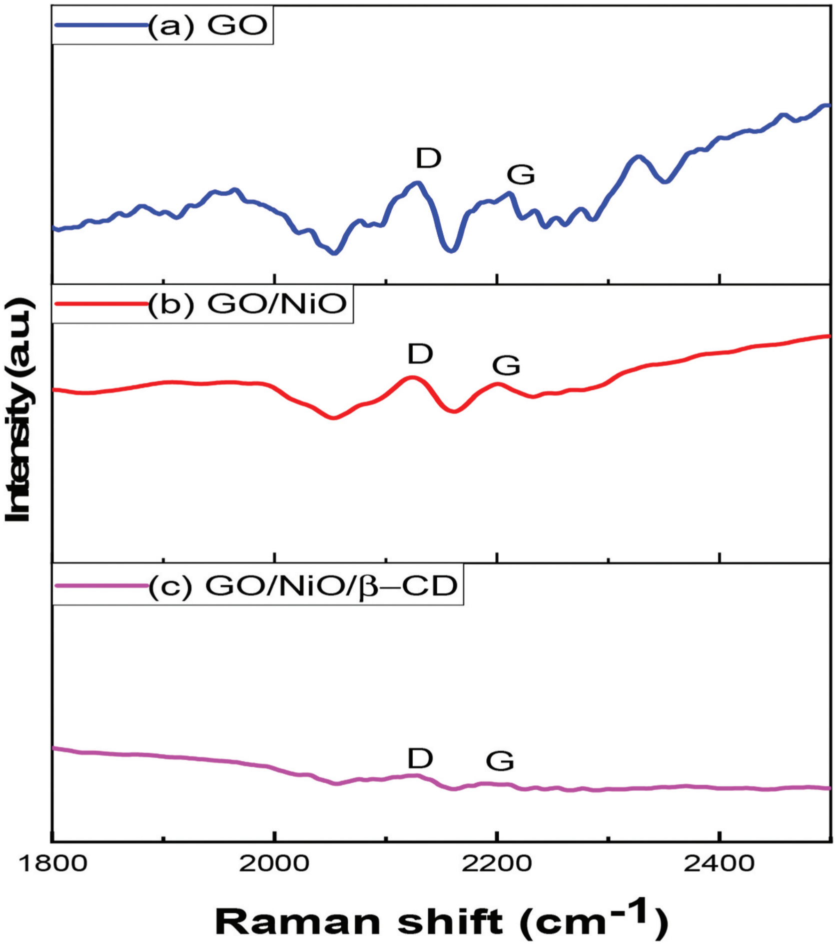

Figure 3. Raman spectrum of (a) GO, (b) GO/NiO and(c) GO/NiO/β-CD.

solutions. Before illumination, the suspensions were continuously stirred in dark for 60 min to reach an adsorption-desorption equilibrium. It could be observed that the GO/NiO/β-CD nanocomposite cannot chemically degrade the dye molecule in dark condition after reaching the adsorption-desorption equilibrium. But, UV-light led to accrue degradation in various extents depending on the catalyst structure. After that, the suspensions were then exposed to natural sunlight irradiation for another 60 min and samples were taken at regular time intervals (0 min to 120 min) and filtered to remove the GO/NiO/β-CD. The same procedure was repeated for MV. The initial pH of solution ~7 was adjusted by small amount of 0.1 M NaOH and 0.1 M HCl. Photodegradation was also studied for 100 ppm MB and MV solution using only GO/NiO/β-CD. The decolourisation efficiency of MB and MV was determined by using the equation:

$$\textit{photodegradation efficiency}(\%) = \left[\frac{A_0 - A_t}{A_0}\right] \times 100\% \tag{3}$$

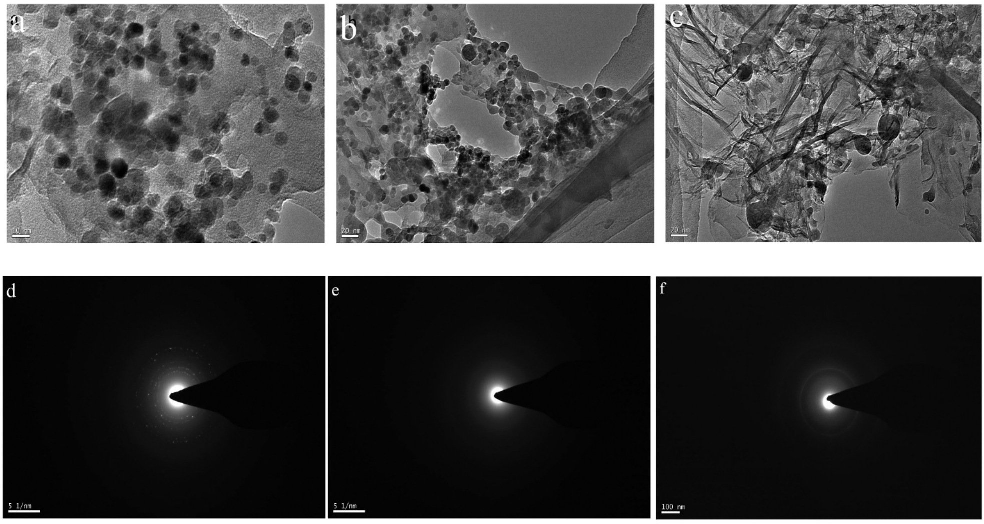

Figure 4. HR-TEM Images of (a) GO, (b) GO/NiO and (c) GO/NiO/β-CD, and SAED patterns of (d) GO, (e) GO/NiO and (f) GO/NiO/β-CD.

Where A_0 is the initial concentration of dye solution and A_t is the final concentration of dye at any time t [12].

UV-vis spectrophotometer was used to measure absorbance of the dye solution at regular time intervals using GO/NiO/β-CD. Controlled experiments were also carried out to confirm the degradation of MB and MV by UV-visible spectra. Under the irradiation of natural sunlight, GO/NiO/β-CD nanocomposites showed 90% (MB) and 69.54% (MV) photodegradation efficiency after 120 min as shown in Figures 5 and 6. Moreover, it is clear from both Figure 7a and b that, GO/NiO/β-CD as expected showed highest photocatalytic activity of MB degradation as compared to MV. The results indicate that β-CD could obviously accelerate the photocatalytic efficiency even in the presence of GO sheets [69].

3.6. Kinetic model

Figures 5 and 6 exhibit the UV-visible spectra of MB and MV dyes at different degradation conditions and time intervals in the wavelength range of 400–700 nm. In Figure 7(a), it is seen that the GO/NiO/β-CD nanocomposite chemically degraded the dye, solar light led to accumulate degradation in various extent depending on the catalyst structure. Figure 7 (b) represents the dependence of dye concentration on reaction time. Photocatalytic degradation reactions are generally explained by a simple 'pseudo-first-order' kinetic equation according to the well-known Langmuir–Hinshelwood model given as

$$\boldsymbol{C_0 = C_t e^{-kt}} \tag{4}$$

$$\boldsymbol{-\ln\frac{C_t}{C_0} = ktm} \tag{5}$$

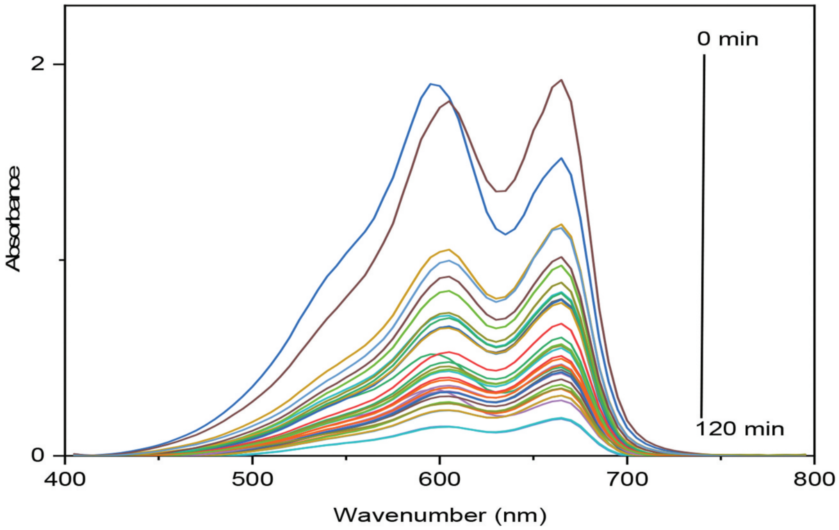

Figure 5. Time-dependent absorption spectra of MB solution during natural sunlight irradiation. Reaction conditions: MB concentration 20 ppm, photocatalyst loading 0.1 g, pH ~7.

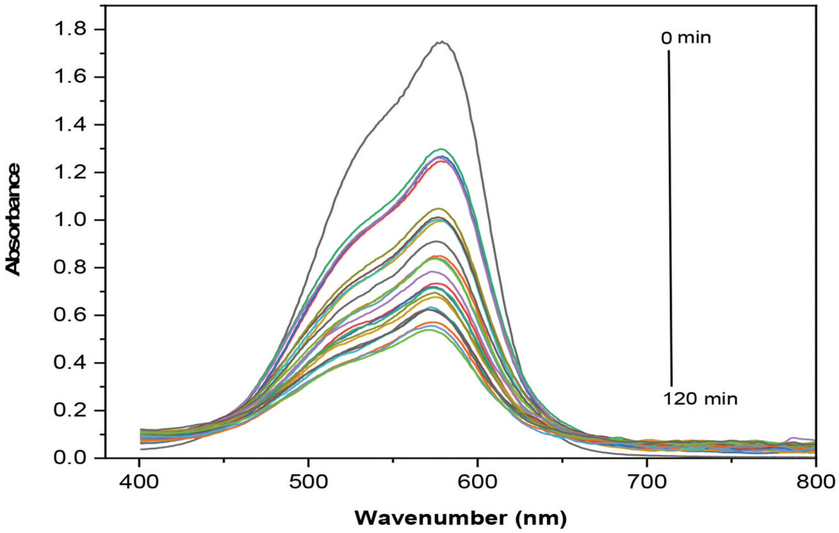

Figure 6. Time-dependent absorption spectra of MV solution during natural sunlight irradiation Reaction conditions: MV concentration 20 ppm, photocatalyst loading 0.1 g, pH ~7.

Where C_0 and C_t are the initial dye concentration and concentration at t, respectively, k is the reaction rate constant (min^{-1}) [70].

The plot of $-\ln(C_t/C_0)$ versus t yields straight lines and the slope of the lines imparts rate constant as seen in Figure 7(b). The calculated values of k, degradation efficiency (%) and correlation coefficient (r^2) are listed in Table 2. As seen in Figure 7(b), reaction data fitted well to pseudo first order kinetic model. Regarding the k and (%) values, it can be

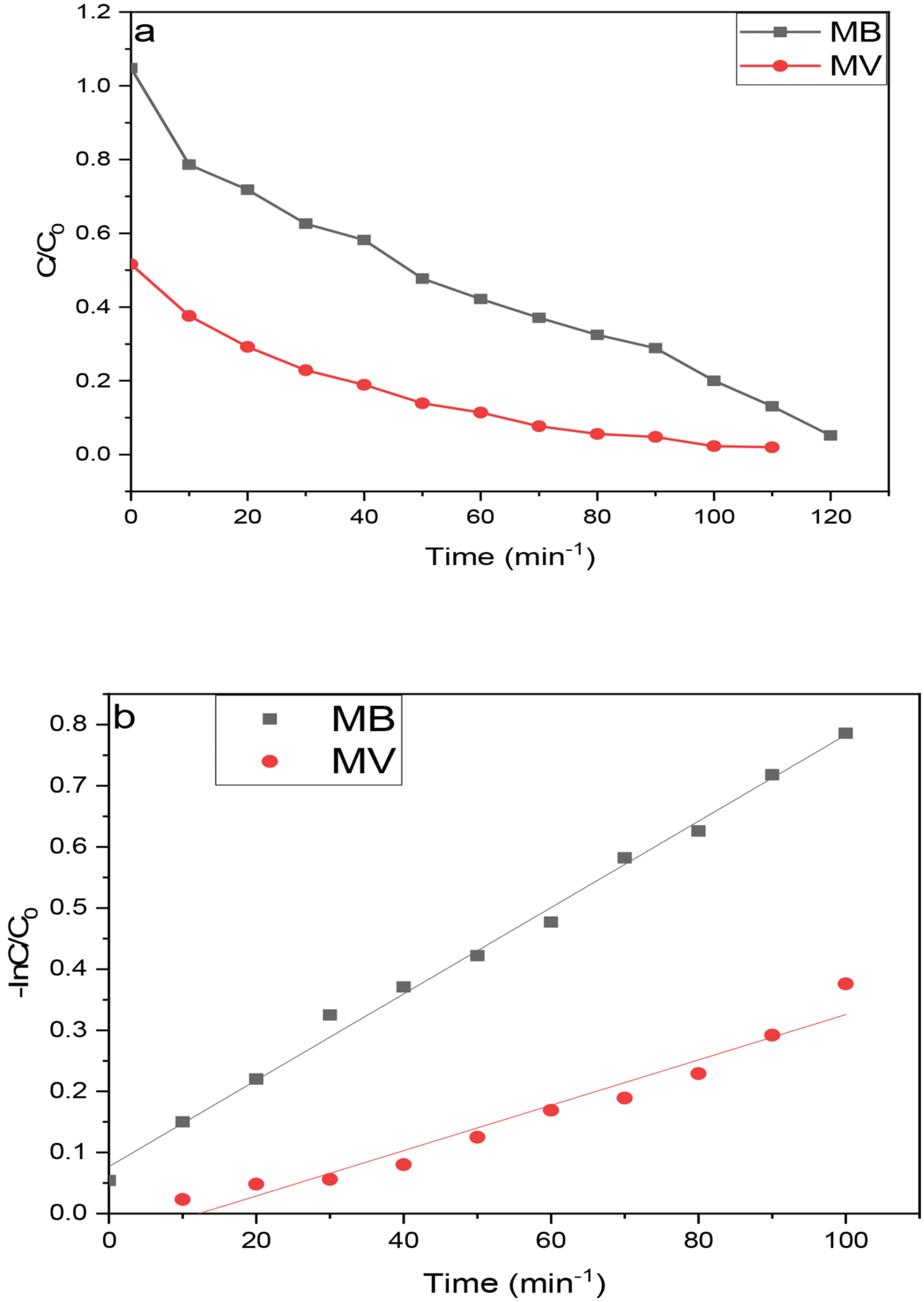

Figure 7. (a) Concentration dependence of MB and MV as a function of time and (b) Langmuir-Hinshelwood (L-H) first-order kinetic model fit at different reaction conditions: MB and MV concentration 20 ppm, photocatalyst loading 0.1 g, pH ~7.

concluded that the GO/NiO/β-CD nanocomposite exhibited a catalytic activity itself under UV light. It might be originated from its acidic nature and reactive oxygen species onto graphitic nanosheets. Photocatalytic efficiency of bulk GO based nanocomposites was found to be higher than MV, as expected. But, the MB dye showed the highest catalytic activity and yielded about a three-fold higher *k* value [71,72].

3.7. Mechanism of photodegradation through GO/NiO/β-CD

Heterogeneous photocatalyst is the best way for dye removal and wastewater treatment to utilise the solar light, and it is a cost-effective technique as well. Heterogeneous Fenton process is generally supported in an aqueous medium and oxidises water molecules into hydroxyl radicals as an active species. AOPs are consuming high energy, produce more iron sludge during Fenton process and have, high operational charge etc, which impede their large-scale application. Metal-oxide-based photocatalysts are photochemically active and non-toxic and consume solar light effectually. Several inorganic nanoparticles such as TiO_2, CuO, ZnO, Bi_2O_3/BiOCl, bimetallic nanoparticles (Pd/Fe), ZnO/$ZnWO_4$ etc. have been proposed for dye removal and water purification [73–75]. Furthermore, heterogeneous Fenton process are efficient method for dye removal which can directly utilise the solar light and degrade the pollutants and produce photo-generated electron hole pairs from reactive oxygen species [76,77]. In the present work, we have synthesised GO/NiO/β-CD nanocomposites and further explored their use for removal of cationic dyes [78,79].

The general mechanism proposed for photocatalytic activity of GO/NiO/β-CD is shown in Figure 8. Firstly cationic dye, MB or MV absorbs the photon and irradiation of light creates the electron and holes. In the second step, composite of GO/NiO/β-CD captures the photogenerated electrons and shifts to the excited dye molecules therefore increases the number of participating excited electron. In the third step, the excited electrons attack the oxygen molecules, which can lead to further generation of hydroxyl

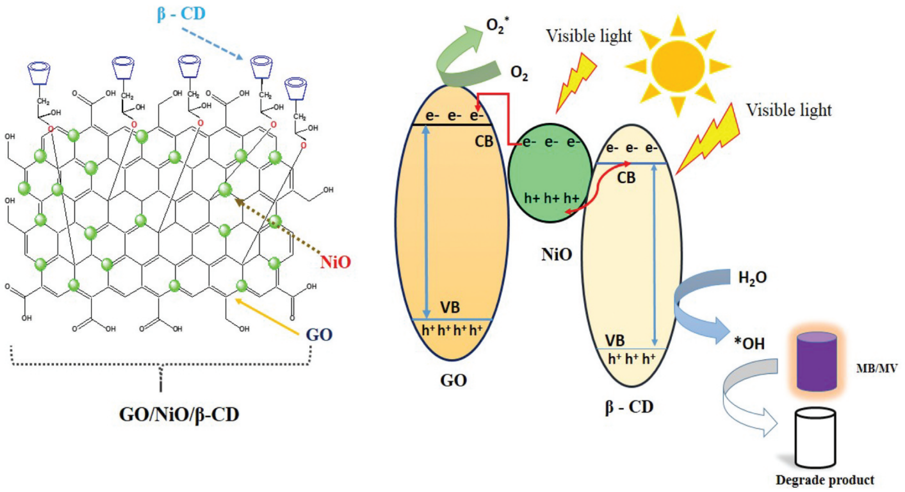

Figure 8. Schematic illustration of GO/NiO/β-CD nanocomposite as a photocatalyst.

radicals and produce H_2O_2. Then this generated H_2O_2 molecules are further confronted by holes and electrons prompting the production of more OH^- and OH* radicals. In the last step the radical species encounter with radical cations of dye molecules which in due course causes its discoloration.

3.8. Investigation on main oxidative species

AOPs involving heterogeneous photocatalysis explain the mechanism of dye degradation. This process involves generation of e^- hole pair. This photogenerated e^- hole pair again generates highly reactive $O_2^{-•}$ and $^•OH$ radicals which are responsible for oxidative mineralisation of the dyes. Again there is generation of hydrogen atoms from water. These are responsible for reductive mineralisation of the dye [80]. It is of great importance to detect main active species in the photocatalysis for elucidation of photocatalytic degradation mechanism of direct dye by GO/NiO/β-CD. Detection can be carried out by using oxidative species trapping experiment, performed under identical conditions. The oxidative species like $^•OH$, h^+ and $O_2^{-•}$ are trapped by using isopropanol (i-PrOH) ($^•OH$ scavenger), methanol (MeOH) ($O_2^{-•}$ scavenger), ethylene diamine tetra acetic acid (EDTA) (h^+ scavenger) and potassium iodide (KI) ($^•OH$ and h^+ scavenger). The photogenerated holes also cause direct oxidation of smaller alcohols like i-PrOH. But as it is negligible, it is neglected. The results in terms of dye degradation by GO/NiO/β-CD using various scavengers are summarised in Figure 9. On addition of MeOH, EDTA, i-PrOH and KI; the photocatalytic degradation of dyes MB and MV decreases down to 83.8, 56.2, 30.5 and

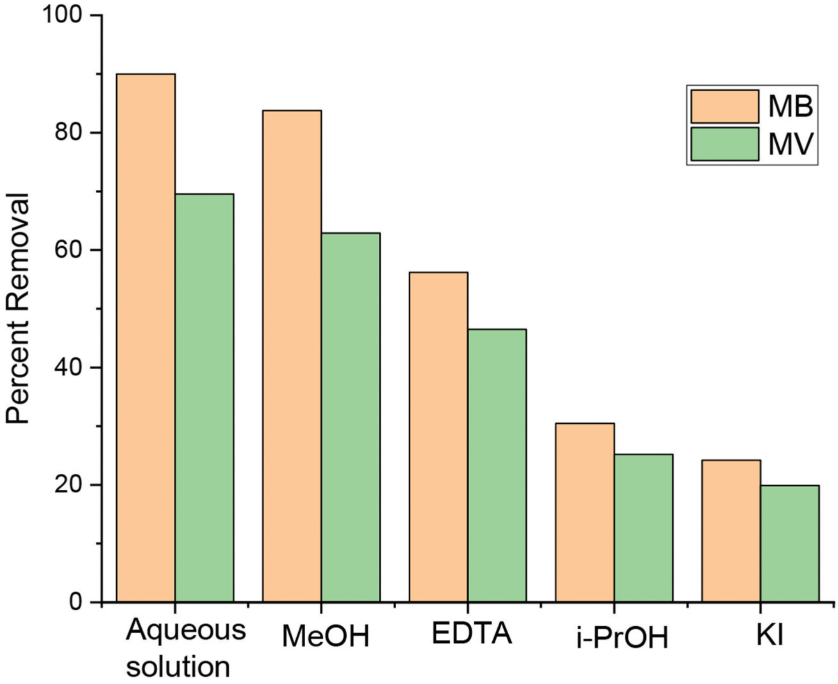

Figure 9. Scavenging study of photocatalytic degradation of MB and MV by GO/NiO/βCD with/without scavenger.

24.2% (MB), respectively as compared to photocatalytic degradation carried out in aqueous medium (90%). From Figure 9 it was observed that, MeOH has very little influence on dye degradation. However, the photocatalytic performance of GO/NiO/β-CD greatly suppressed by addition of $^{\bullet}$OH and h^+ scavenger (KI), suggesting that the photogenerated holes and $^{\bullet}$OH are the predominant species of GO/NiO/β-CD whereas, the O_2 radical assists in the degradation of dye under natural sun light irradiation.

3.9. Recycle performance of GO/NiO/β-CD nanocomposite

Stability of the GO/NiO/β-CD nanocomposite was confirmed by reusability of the GO/NiO/β-CD in the photocatalytic degradation of dyes (MB and MV) under exposure of natural sun light irradiation. To study its reusability, after photocatalytic degradation the powdered nanocomposite was allowed to settle by gravity and then separated. The recovered nanocomposite was collected and then recycled for 3 times under same photocatalytic experimental conditions. Removal of MB and MV by GO/NiO/β-CD after 1st cycle achieved upto 90% (MB) and 69.54% (MV). It decreases down to 85.5%, 81.7%, 76.5% (MB) and 65.2%, 59.8%, 45.3% (MV), and after 2nd, 3rd and 4th cycles respectively as shown in Figure 10. Thus it reveals that GO/NiO/β-CD has excellent stability and does not show significant loss in activity after four cycles. It should be noted that decrease in percent removal of dye was due to loss of recycled catalyst during sampling each time. This reveals that GO/NiO/β-CD does not photo-corrode during photocatalytic degradation.

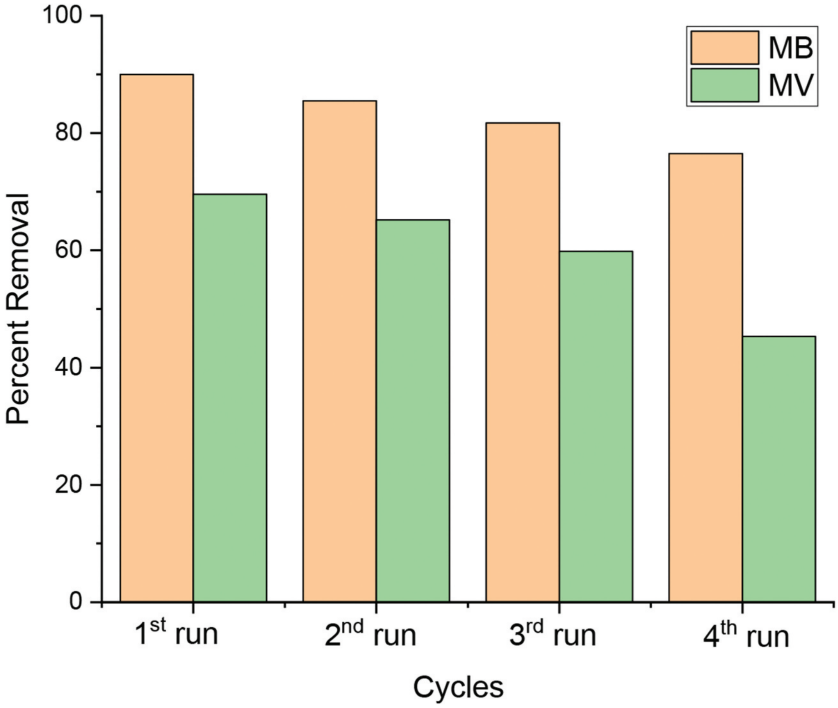

Figure 10. Recycling performance of the GO/NiO/β-CD.

This exhibits the practical applicability of GO/NiO/β-CD with higher photocatalytic performance for the degradation of MB dye [81].

4. Conclusion

GO/NiO/β-CD nanocomposites with an average particle size 1–10 nm could be successfully synthesised via a facile and simple hydrothermal method. Raman spectra suggest a decrease in the average size of the sp^2 domains from GO/NiO/β-CD composite and confirm formation of new graphitic domains after the oxidation process. From the HR-TEM images of GO/NiO/β-CD nanocomposite, it can be concluded that β-CD has been modified on the surface of GO through covalent bonding. GO/NiO/β-CD shows significant enhancement in photocatalytic degradation of dye under light irradiation as compared to MB and MV dyes. Percent removal of dye achieved by MB was 90% whereas by MV it was 69.54%. Improvement in photocatalytic performance of GO/NiO/β-CD was due to reduction in recombination of photogenerated e^--hole pair and their transfer by GO sheets as well as combined effect of adsorption and photocatalysis of GO/NiO/β-CD. The photodegradation followed Langmuir-Hinshelwood kinetic model. The scavenger study shows that h^+ and •OH radicals are the predominant species in the photocatalytic mineralisation of dye in comparison with O_2. This suggests the oxidative mineralisation. Furthermore, the GO/NiO/β-CD nanocomposite with high mineralisation efficiency, stability and recyclability could be potential material for wastewater treatment.

Acknowledgements

The authors are grateful to Sophisticated Analytical Instruments Facility, Cochin (India), NIT Raipur and IIT Madras for FTIR, XRD, Raman spectra and HR-TEM analysis. The authors would also like to thank DST-FIST (New Delhi) sponsored by Department of Chemistry.

Disclosure statement

The authors declare no conflict of interest

ORCID

Ajaya K. Singh http://orcid.org/0000-0001-8180-7292

References

[1] X.Z. Tang, Z. Cao, H.B. Zhang, J. Liu and Z.Z. Yu, Chem. Commun. **47**, 3084 (2011). doi:10.1039/C0CC05613H.

[2] H.J. Arvind and K. Hern, J. Adv. Res. **622**, 827 (2013). doi:10.4028/www.scientific.net/AMR.622-623.827.

[3] M. Vinothkanan, C. Karthikeyan, G. Gnanakumar, A.R. Kim and D.J. Yoo, Spectrochim. Acta A Mol. Biomol. Spectrosc. **136**, 256 (2015). doi:10.1016/j.saa.2014.09.031.

[4] M. Anas, D.S. Han, K. Mahmoud, H. Park and A. Abdel-Wahab, Mat. Sci. Semicond. Proc. **41**, 209 (2015). doi:10.1016/j.mssp.2015.08.041.

[5] M. Salavati-Niasari, Chem. Lett. **34**, 1444 (2005). doi:10.1246/cl.2005.1444.

[6] M. Avila, T. Burks, F. Akhtar, M. Göthelid, P.C. Lansåker, M.S. Toprak, M. Muhammed and A. Uheida, Chem. Eng. J. **245**, 201 (2014). doi:10.1016/j.cej.2014.02.034.

[7] M. Sabet, M. Salavati-Niasari and O. Amiri, Electrochim. Acta **117**, 504 (2014). doi:10.1016/j.electacta.2013.11.176v.

[8] H. Si, T. Wang and Z. Xu, Wood Sci. Technol. **47**, 1177 (2013). doi:10.1007/s00226-013-0567-2.

[9] Y.V.V. Aswani Kumar, R.M. Renuka, J. Achuth, V. Mudili and S. Poda, RSC Adv. **8**, 10465 (2018). doi:10.1039/c8ra00317c.

[10] J.W. Ong, J.J. Yeong, L.L. Tan, B.T. Goh, S.T. Yong and S.P. Chai, RSC Adv. **4**, 59676 (2014). doi:10.1039/C4RA10467F.

[11] M. Salavati-Niasari, M.R. Loghman-Estarki and F. Davar, Chem. Eng. J. **145**, 346 (2008). doi:10.1016/j.cej.2008.08.040.

[12] N. SheibaniTezerji, M. Mehdi Foroughi, R. Rezaei Bezenjani, N. Jandaghi, E. Rezaeipour and F. Rezvani, Food Chem. **311**, 125747 (2020). doi:10.1016/j.foodchem.2019.125747.

[13] S.H.S. Chan, Y.T. Wu, J.C. Juan and C.Y. Teh, J. Chem. Technol. Biotechnol. **86**, 1130 (2011). doi:10.1002/jctb.2636.

[14] W. Zhang, B.S. Naidu, J.Z. Ou, A.P. O'Mullane, A.F. Chrimes, B.J. Carey, Y. Wang, S.Y. Tang, V. Sivan and A. Mitchell, ACS Appl. Mater. Interfaces **7**, 1943 (2015). doi:10.1021/am5077364.

[15] M. Salavati-Niasari, Micropor. Mesopor. Mat. **95**, 248 (2006). doi:10.1016/j.micromeso.2006.05.025.

[16] Y. Lei, F. Chen, Y. Luo and L. Zhang, Chem. Phys. Lett. **593**, 122 (2014). doi:10.1016/j.cplett.2013.12.066.

[17] M. Salavati-Niasari, D. Ghanbari and M.R. Loghman-Estarki, Polyhedron **35**, 149 (2012). doi:10.1016/j.poly.2012.01.010.

[18] K. Sahel, N. Perol, H. Chermette, C. Bordes, Z. Derriche and C. Guillard, Appl. Catal. B Environ. **77**, 100 (2007). doi:10.1016/j.apcatb.2007.06.016.

[19] M. Mitra, A. Ghosh, A. Mondal, K. Kargupta, S. Ganguly and D. Banerjee, Appl. Surf. Sci. **402**, 418 (2017). doi:10.1016/j.apsusc.2017.01.072.

[20] R.S. Dariani, A. Esmaeili, A. Mortezaali and S. Dehghanpour, Optik **127**, 7143 (2016). doi:10.1016/j.ijleo.2016.04.026.

[21] T. Soltani and M.H. Entezari, J. Mole. Cat. **377**, 197 (2013). doi:10.1016/j.molcata.2013.05.004.

[22] S. Kansal, N. Kaur and S. Singh, Nanoscale Res. Lett. **4**, 709 (2009). doi:10.1007/s11671-009-9300-3.

[23] G. Wang, F. Wu, X. Zhang, M. Luo and N. Deng, Hazard Mater **133**, 85 (2006). doi:10.1016/j.jhazmat.2005.09.058.

[24] Y. Zhang, Z. Chen, L. Zhou, P. Wu, Y. Zhao and Y.L. Fei, Environ. Pollut. **244**, 93 (2019). doi:10.1016/j.envpol.2018.10.028.

[25] M. Salavati-Niasari, M. Shaterian, M.R. Ganjali and P. Norouzi, J. Mol. Catal. A: Chem. **261**, 147 (2007). doi:10.1016/j.molcata.2006.07.048.

[26] J.X. Jiao, K. Du, Y. Wang, P. Sun, H. Zhao, P. Tang, Q. Fan, H. Tian, Q. Li and Q. Hu, Mater. Chem. Phys. **240**, 122169 (2020). doi:10.1016/j.matchemphys.2019.122169.

[27] X. Kang, X. Zhu, J. Liu, X. Shu, Y. Huang and J. Qian, Compos. Part B Eng. **186**, 107800 (2020). doi:10.1016/j.compositesb.2020.107800.

[28] S.H. Choi and Y.C. Kang, Chem. Sus. Chem. **7**, 523 (2014). doi:10.1002/cssc.201300838.

[29] S.J. Chin, M. Doherty, S. Vempati, P. Dawson, C. Byrne, B.J. Meenan, V. Gueera and T. McNally, Nanoscale **11**, 18672 (2019). doi:10.1039/C9NR04202D.

[30] O. Rabbani, S. Ghasemi and S.R. Hosseini, J. Alloys Compd. **840**, 155665 (2020). doi:10.1016/j.jallcom.2020.155665.

[31] K. Zhang, M. Ye, A. Han and J. Yang, J. Solid State Chem. **277**, 68 (2019). doi:10.1016/j.jssc.2019.05.046.

[32] F. Davar, M. Salavati-Niasari, N. Mir, K. Saberyan, M. Monemzadeh and E. Ahmadi, Polyhedron **29**, 1747 (2010). doi:10.1016/j.poly.2010.02.026.

[33] F. Motahari, M.R. Mozdianfard, F. Soofivand and M. Salavati-Niasari, J. Name. 2012, 1. doi:10.1039/C4RA02697G

[34] M.A. Moharrama, K.M.T. Ereiba, W. El Hotabya and A.M. Bakr, React. Funct. Polym. **101**, 9 (2016). doi:10.1016/j.reactfunctpolym.2016.02.001.

[35] N. Sun, T. Wang and C. Liu, Wood Sci. Technol. **50**, 1243 (2016). doi:10.1007/s00226-016-0826-0.

[36] S.S. Ray and M. Bousmin, Prog. Mater. Sci. **50**, 962 (2005). doi:10.1016/j.pmatsci.2005.05.002.

[37] P.M. Navajas, N.G. Asenjo, R. Santamaria, R. Menendez, A. Corma and H. Garcia, Langmuir **29**, 13443 (2013). doi:10.1021/la4029904.

[38] K.M. Reza, A.S.W. Kurny and F. Gulshan, Int. J. Env. Sci. Dev. **7**, 325 (2016). doi:10.7763/IJESD.2016.V7.793.

[39] M. Shanmugam and R. Jayavel, J. Nanosci. Nanotechno. **15**, 7195 (2015). doi:10.1166/jnn.2015.10562.

[40] R. Pasricha, S. Gupta and A.K. Srivastava, Small **5**, 2253 (2009). doi:10.1002/smll.200900726.

[41] L. Jiang, Y. Liu, S. Liu, X. Hu, G. Zeng, X. Hu, S. Liu, S. Liu, B. Huang and M. Li, Chem. Eng. J **308**, 597 (2017). doi:10.1016/j.cej.2016.09.067.

[42] P. Tan and Y. Hu, J. Mol. Liq. **167**, 31943 (2017). doi:10.1016/j.molliq.2017.07.010.

[43] H. Fan, X. Zhao, J. Yang and X. Shan, Catal. Commun. **29**, 29 (2012). doi:10.1016/j.catcom.2012.09.013.

[44] C. Puri and G. Sumana, Appl. Clay Sci. **116**, 102 (2018). doi:10.1016/j.clay.2018.09.012.

[45] S. Janani, K.S. Rani Sudha, E. Padmini and R.M. Lima, J. Environ. Chem. Eng. **4**, 534 (2016). doi:10.1016/j.jece.2015.10.043.

[46] G. Wang, W. Fan, Q. Li and N. Deng, Chemosphere **216**, 707 (2019). doi:10.1016/j.chemosphere.2018.10.199.

[47] A. Hashmi, A.K. Singh, B. Jain and S.A.C. Carabineiro, Nanomaterials **10**, 105 (2020). doi:10.3390/nano10010105.

[48] L. Wang, H. Xing, S. Gao, X. Ji and Z. Shen, Mater Chem. C **5**, 2005 (2017). doi:10.1039/C6TC05179K.

[49] M.D.H. Beg, A.K.M. MoshiulAlam, R.M. Yunus and M.F. Mina, J. Nanoparticle Res. **17**, 53 (2015). doi:10.1007/s11051-014-2846-8.

[50] Z. Zhou, H. Ni and L.Z. Fan, J. Nanosci. Nanotechnol. **14**, 1533 (2014). doi:10.1166/jnn.2014.8685.

[51] S. Mahpishanian and H. Sereshti, J. Chromatogr. A **1485**, 32 (2017). doi:10.1016/j.chroma.2017.01.035.

[52] Y. Xu, H. Bai, G. Lu, C. Li and G. Shi, J. Am. Chem. Soc. **130**, 5856 (2008). doi:10.1021/ja800745y.

[53] S. Verma, H.P. Mungse, N. Kumar, S. Choudhary, S.L. Jain, B. Sain and O.P. Khatri, Chem. Commun. **47**, 12673 (2011). doi:10.1039/C1CC15230K.

[54] L. Fan, C. Luo, M. Sun, H. Qui and X. Li, Colloids Surf. B **103**, 601 (2013). doi:10.1016/j.colsurfb.2012.11.023.

[55] R.P. Liang, C.M. Liu, X.Y. Meng, J.W. Wang and J.D. Qiu, J. Chromatogr. A **1266**, 95 (2012). doi:10.1016/j.chroma.2012.09.101.

[56] Y. Zhu, W. Chu, N. Wang, T. Lin, W. Yang, J. Wen and X.S. Zhao. J. Name. **1** (2015). doi:10.1039/C5RA14790E.

[57] H. Wu, W. Zhao, H. Hu and G.J. Chen, Mater Chem. **21**, 8626 (2011). doi:10.1039/C1JM10819K.

[58] J. Ge, Y. Hu, M. Biasini, W.P. Beyermann and Y. Yin, Angew. Chem. Int. Ed. **46**, 4342 (2007). doi:10.1002/anie.200700197.

[59] L.Z. Bai, D.L. Zhao, Y. Xu, J.M. Zhang, Y.L. Gao, L.Y. Zhao and J.T. Tang, Mater. Lett. **68**, 399 (2012). doi:10.1016/j.matlet.2011.11.013.

[60] C. Hou, Q. Zhang, M. Zhu, Y. Li and H. Wang, Carbon **49**, 47 (2011). doi:10.1016/j.carbon.2010.08.040.

[61] B. Konkena and S. Vasudevan, Langmuir **28**, 12432 (2012). doi:10.1021/la3020783.

[62] N.V. Hoan, N.N. Minh, T.T. Kim Nhi, N.V. Thang, V.A. Tuan, V.T. Nguyen, N.M. Thanh, N.V. Hung and D.Q. Khieu, J. Nanomater. **2020**, 3 (2020). doi:10.1155/2020/4350125.

[63] F.V. Ferreiraa, F.S. Britoa, W. Franceschia, E.A.N. Simonettic, L.S. Cividanesa, M. Chiparad and K. Lozanob, J. Surf. Interfac. **10**, 100 (2018). doi:10.1016/j.surfin.2017.12.004.

[64] G.M. Neelgund, A. Oki and Z. Luo, Mater. Res. Bull. **48**, 175 (2013). doi:10.1016/j.materresbull.2012.08.077.

[65] C.N. Huy, N. Kim, T.D.N. Phan, I.K. Yoo and E.W. Shin, Nanoscale Res. Lett. **9**, 462 (2014). doi:10.1186/1556-276X-9-462.

[66] B.P. Nenavathu, S. Kandula and S. Verma, RSC Adv. **8**, 19659 (2018). doi:10.1039/c8ra02237b.

[67] H. Wang, Y.G. Liu, G.M. Zeng, X.J. Hu, X. Hu, T.T. Li, H.Y. Li, Y.Q. Wang and L.H. Jiang, Carbohydr. Polym. **113**, 166 (2014). doi:10.1016/j.carbpol.2014.07.014.

[68] J. Liu, G. Liu and W. Liu, Chem. Eng. J. **257**, 299 (2014). doi:10.1016/j.cej.2014.07.021.

[69] G.R. Bardajee, S.S. Hosseini and C. Vancaeyzeele, New J. Chem. **43**, 3572 (2019). doi:10.1039/C8NJ05800H.

[70] N. Zhang, M.Q. Yang, S. Liu, Y. Sun and Y.J. Xu, Chem. Rev. **115**, 10307 (2015). doi:10.1021/acs.chemrev.5b00267.

[71] M. Minella, F. Sordello and C. Minero, Catal. Today. **281**, 29 (2017). doi:10.1016/j.cattod.2016.03.040.

[72] S. Kang, M. Pinault, L.D. Pfefferle and M. Elimelech, Langmuir **23**, 8670 (2007). doi:10.1021/la701067r.

[73] A.R. Chowdhuri, S. Tripathy, C. Haldar, S. Chandra, B. Das, S. Roy and S.K. Sahu, RSC Adv. **5**, 21515 (2015). doi:10.1039/C4RA16785F.

[74] X. Pan, Y. Wang, Z. Chen, D. Pan, Y. Cheng, Z. Liu and X. Guan, ACS Appl. Mater. Interfaces **5**, 1137 (2013). doi:10.1021/am302910q.

[75] C. Hu, X. Hu, J. Guo and J. Qu, Environ. Sci. Technol. **40**, 5508 (2006). doi:10.1021/es052405v.

[76] J.C. Yu, W. Ho, J. Yu, H. Yip, P.K. Wong and J. Zhao, Environ. Sci. Technol. **39**, 1175 (2005). doi:10.1021/es035374h.

[77] K. Lu, G. Zhao and X. Wang, Chin. Sci. Bull. **57**, 1223 (2012). doi:10.1007/s11434-012-4986-5.

[78] T.S. Sreeprasad and T. Pradeep, Int. J. Mod. Phys. B **26**, 1242001 (2012). doi:10.1142/S0217979212420015.

[79] S. Meshram, R. Limaye, S. Ghodke, S. Nigam, S. Sonawanw and R. Chikate, Chem. Eng. J. **172**, 1008 (2011). doi:10.1016/j.cej.2011.07.015.

[80] S.P. Patil, R.P. Patil, V.K. Mahajan, G.H. Sonawane, V.S. Shrivastava and S. Sonawanw, Mater. Sci. Semicond. Process. **52**, 55 (2016). doi:10.1016/j.mssp.2016.05.008.

[81] J. Ahmad and K. Majid, Adv. Compos. Mater. **1**, 374 (2018). doi:10.1007/s42114-018-0025-6.